Local-scale analysis of the longitudinal strains in strongly necking materials by means of video-controlled extensometry

1994 J. Phys.: Condens. Matter 6 8959

(http://iopscience.iop.org/0953-8984/6/42/025)

J. Phys.: Condens. Matter 6 (1994) 8959–8968. Printed in the UK

Local-scale analysis of the longitudinal strains in strongly necking materials by means of video-controlled extensometry*

Ph François, V Gaucher and R Séguéla

Laboratoire 'Structure et Propriétés de l'Etat Solide', URA CNRS 234, Bâtiment C6, Université de Lille 1, 59655 Villeneuve d'Ascq Cédex, France

Received 4 July 1994

Abstract. A novel method of determination of the longitudinal strains at a very local scale in the case of materials that develop a plastic neck under tensile drawing is presented. It relies on the analysis of the distortions of a linear target drawn on a thick thermoplastic polymer film by means of computer-assisted video-controlled extensometry. An equation is given for the target slope as a function of the local principal strains. True-stress and true-strain determinations can be performed along the neck as it forms and propagates. *In situ* measurements of the volume variations are afforded as a function of strain during the necking process

1. Introduction

The determination in real time of the local deformations in materials which exhibit plastic instability has been long a matter of preoccupation. Indeed, true-stress and true-strain measurements are required for study of the thermal activation of plasticity as well as for setting up constitutive equations for the plastic flow. G'Sell and coworkers [1–4] have greatly contributed to this task in elaborating several pieces of equipment for the study of glassy and semi-crystalline polymers under uniaxial drawing, simple shear or plane-strain tensile deformation.

A computed-assisted video-monitored extensometer provided with two cameras has been recently developed in our laboratory [5], on the basis of the device contrived by G'Sell *et al* [3]. This equipment was initially assigned to investigating the plastic deformation of glassy polymers under tensile loading and notably the transition between the shear banding and the crazing deformation modes, thanks to an accurate measurement of the longitudinal and transverse strains together with the volume strain.

The present paper deals with a novel method of analysis that allows longitudinal-strain measurements at a very local scale in strongly necking-prone materials. The usefulness of the method is illustrated through the study of a high-density ethylene copolymer which exhibits a marked propensity for plastic instability accompanied with strong whitening upon tensile drawing.

* First presented at the *Institute of Materials Conference on Deformation Yield and Fracture of Polymers (Cambridge, 1994).*

0953-8984/94/428959+10$19.50

2. Experimental method

The previously described optical extensometer [5] is composed of two CCD (charge-coupled device) video cameras equipped with zoom lenses. The front and side views of the sample are digitized into 512 × 512 pixel images, and subsequently processed for further calculations, by means of a Matrox MVP-AT video interface board and a Compaq 386–25 MHz microcomputer. The present method of investigation involves the use of a linear target about 5 mm long in the z tensile axis, inclined with respect to this axis in the region of the minimum width of flat hourglass-shaped samples.

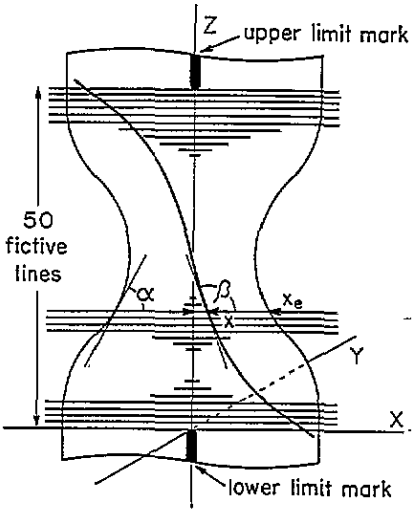

Figure 1. Schematic principle of analysis of the local longitudinal strain from the distortions of the target in the necked region of the sample front image.

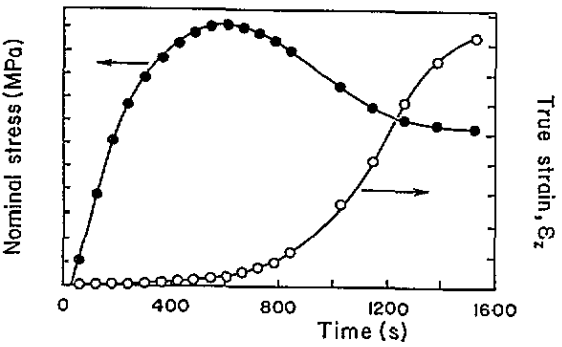

Figure 2. Nominal stress and true strain as a function of time of drawing.

The principle of the analysis of the local deformation along the neck is depicted in the scheme of figure 1 which shows the front view of the sample together with the distorted target and the marks limiting the vertical range of the analysis. The digitized front image, initially enlarged to about 150 pixels between the limiting marks in the z axis, is divided into 50 fictive equidistant horizontal lines. The (x, z) coordinates of the intersections of every line with the target and the sample edges are recorded into files at time intervals varying between 8 s and 60 s, depending on the cross-head speed. The local longitudinal strain, ϵ_z, can be then calculated from the following equation, whose demonstration is provided in the appendix:

$$\frac{\tan \beta_0}{\tan \beta} - \frac{\tan \beta_0}{\tan \alpha} \frac{x}{x_e} = \frac{1+\epsilon_x}{1+\epsilon_z}. \tag{1}$$

At any z ordinate in the neck, the target abscissa, x, is taken at mid-breadth of the target line while the edge abscissa, x_e, is determined from the half width of the neck. The transverse strain, ϵ_x, is calculated from the change in width of the sample all along the target range. $\tan \beta_0$ is the slope of the target prior to deformation, with β_0 lying in practice in the range 135–150°.

The slope of the distorted target with respect to the x axis, $\tan \beta$, is determined numerically from a fitting procedure based on the propagation of a second-order polynomial regression over ten consecutive data of the experimental (x, z) coordinate files. It is to be mentioned that this procedure has been adopted after unsuccessful tries at fitting with many different functions. Propagation consists in taking routinely into account an additional point forward in a data file and withdrawing the first of the ten points of the preceding polynomial fit calculation. A first determination of rough $\tan \beta$ values is made by taking into account the computed value of the polynomial derivative at mid-distance of the z interval of every fit along the target. A smoothing of these rough $\tan \beta$ data is performed owing to an additional fit procedure involving the propagation of a second-order polynomial regression analogous to the previous one but, in this case, the smoothed $\tan \beta$ values are directly taken from the polynomial value at mid-distance of the z interval of every fit performed on the rough $\tan \beta$ data.

The slope of the sample edge with respect to the x axis, $\tan \alpha$ is assessed from the sample edge coordinates of the experimental data files following a two-step fit procedure similar to the one used for the determination of $\tan \beta$.

For the sake of simplification, and taking into account the large radius of curvature of the hourglass constriction of the sample, the gauge profile prior to deformation can be assumed linear in the range of the target. The deviation from linearity in indeed less than 2%.

The relevance of the local longitudinal-strain deformation can be checked out through the following test:

$$\int \epsilon_z \mathrm{d}z = \epsilon_z \tag{2}$$

which means that integration of the local strain, ϵ_z over the whole range of analysis between the limit marks should be equal to the average strain, $\epsilon_z = L/L_0$, L and L_0 being the distances between the marks at a given time of the drawing and prior to the drawing, respectively. In practice, the test agreement is usually better than 5%. This result provides strong confidence in the present method of strain analysis.

In order to check the deformation isotropy in the sample cross-section during the drawing process, the transverse strain, ϵ_y, within the sample thickness is also determined at the minimum width of the neck, using the digitized image of the sample side view.

Considering the optical magnification used for the present experiments, the resolution of the digitized images is about 30 μm per pixel. The resulting absolute accuracy in the ϵ_x and ϵ_y strains is about 5×10^{-3} and 10^{-2}, respectively. As concerns ϵ_z, only an estimated relative accuracy of 5% can be provided on account of the fitting procedures involved in the calculation (see section 4). It is worth noticing that this estimation is consistent with the test agreement of (2).

Nominal stress, σ_N, and true stress, σ_T, data are afforded for every strain value by the computing program which records the load applied on the sample. The stress calculations are performed from the equations

$$\sigma_N = F/S_0 \tag{3}$$

and

$$\sigma_T = \sigma_N/\left[(1+\epsilon_x)(1+\epsilon_y)\right] \tag{4}$$

F being the force applied to the sample and S_0 the initial sample section prior to deformation. Stress triaxiality effects [6] are neglected in a first approximation.

Local volume strains can be also computed from the strains in the three principal axes according to

$$\Delta V/V = (1+\epsilon_x)(1+\epsilon_y)(1+\epsilon_z) - 1. \tag{5}$$

A tentative estimation of the volume-strain error is proposed using the distribution of ten data of the $\Delta V/V$ versus x profile in the central part of the neck, considering that ϵ_z and ϵ_x change very little in this region. This approach takes into account the confidence interval for all data rather than the cumulated error from the three principal strains involved in (5).

3. Material preparation and drawing experiments

The material used in this investigation was an ethylene–butene random copolymer having a density ρ = 0.950 g cm^{-3}, i.e. a crystal weight fraction X_c = 0.70. Its number and weight-average molar weights were M_n = 30 000 and M_w = 157 000, respectively. Sheets about 3 mm thick were compression moulded from pellets at 190 °C and slowly cooled at about 20 ° min^{-1}.

The hourglass-shaped test pieces with dumbell-like ends [5] designed for clamping were cut out from the sheets by means of a cutting die. The curvature radius of the gauge was 58 mm and the minimum width was 6 mm. The limiting marks together with the original target consisting of a straight line about 5 mm long and 0.5 mm large were drawn with a rubbery ink which remained highly deformable after drying in order that they could follow the large deformation of the sample in the neck without unsticking from the sample surface.

Particular attention has been paid to the sample lighting and positioning with respect to the cameras for a proper recording of the target and the sample edge coordinates as well as the sample thickness from the digitized images of the front and side views of the sample.

The drawing experiments have been conducted on a screw-driven Instron testing machine at a constant cross-head speed of 0.5 mm min^{-1}, at room temperature.

4. Video data and treatment

Figure 2 shows the nominal stress and the true strain computed according to the above method as a function of time during the course of the drawing.

An example is given in figure 3 of the raw video data of the target and the neck-width profiles recorded at the time t = 1380 s of the drawing experiment. The dispersion of the data is mainly due to the discrete nature of the measurements having an accuracy of ±1 pixel. Also given in figure 3 are the computed coordinate data of the points at the mid-z range of every polynomial fit from which are calculated the slopes of the target and the neck. These latter data are shown in order to bear witness to the good quality of the first fitting procedure on both profiles. The corresponding tan β and tan α values reported in figure 4 exhibit significant dispersion. These 'rough' data require further refinement before processing to ϵ_z calculations. The second fitting procedure then gives 'smoother' tan β and tan α data that are also shown in figure 4.

From the dispersion of the data, notably in tan β which is the most important parameter of the ϵ_z determination, one may assess a maximum relative error of about 20% on the highest ϵ_z values in the central region of the neck where tan β is very high. But considering the small scatter of the computed ϵ_z values over the whole time range of the investigation (figure 2), the confidence interval on every ϵ_z datum can be reduced to less than 5%.

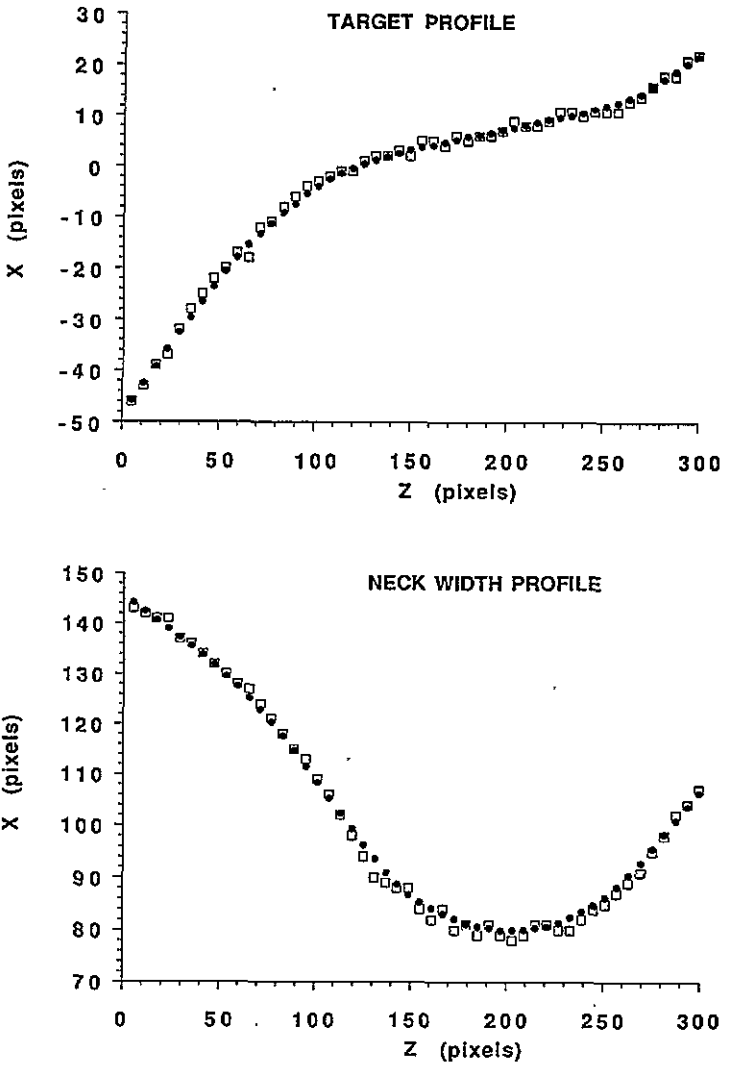

Figure 3. Raw video coordinate (□) of the target and the neck-width profiles recorded at the time t = 1380 s of the drawing experiment and computed coordinate data of the points at the mid-z range of the polynomial fits (●).

5. Results and discussion

The nominal stress and the true strain are reported in figure 2 as a function of time during the course of the drawing. The fairly linear variation of ϵ_z up to the yield point shows that the deformation is nearly homogeneous in the range $0 < \epsilon_z < 0.10$. On the other hand, the marked acceleration in the strain variation beyond the yield point clearly discloses the concentration of the deformation, that is neck initiation. The true strain rate of the necking process can be assessed from the slope of the true-strain–time curve. Plastic deformation in the neck seems to stabilize with the occurrence of the nominal-stress plateau.

The true-stress–true strain curve of figure 5 does not show any drop of the true stress beyond the yield point, i.e. *no intrinsic softening effect. This is perfectly consistent with* the previous studies of G'Sell *et al* [2,3]. The Considere construction [7] confirms that

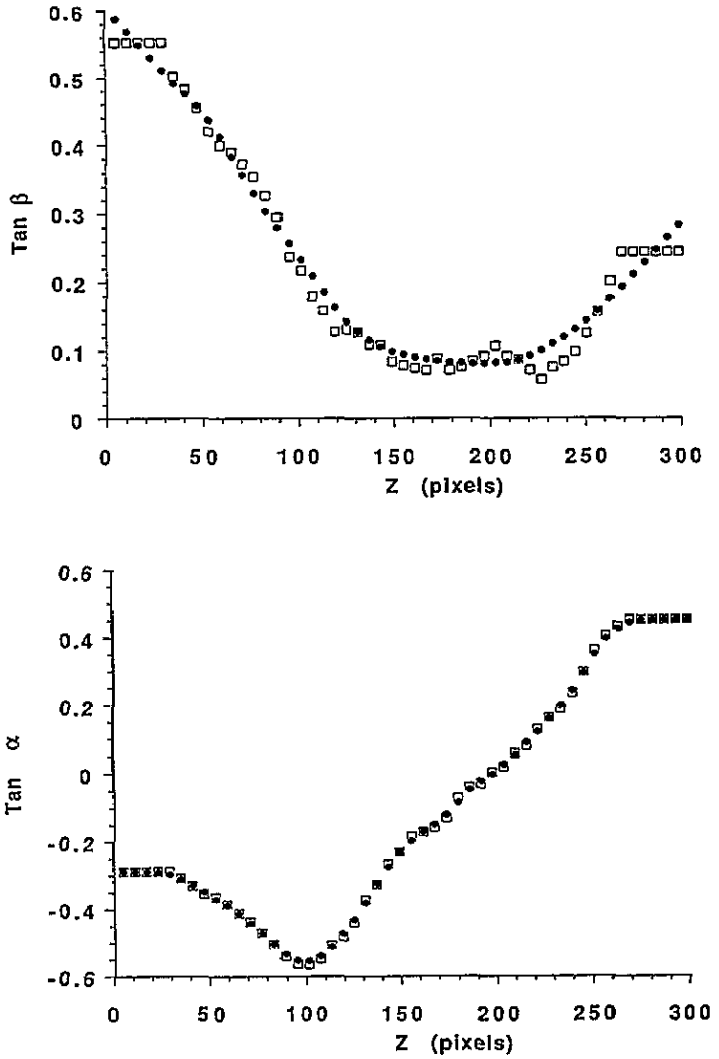

Figure 4. Rough tan β and tan α data (□) calculated from the derivatives of the polynomials of the first fitting procedure performed on the raw coordinates of the target and the neck-width profile, and smoother tan β and tan α values (●) obtained from the polynomial values of the second fitting procedure performed on the former rough tan β and tan α data.

plastic deformation stabilizes at about $\epsilon_z = 4$.

The volume strain as a function of time is shown in figure 6. It is obvious that the present method of strain measurement is unable to detect the volume variations in the material before the yield point. Indeed, elastic volume strains are usually a few per cent only, i.e. of the same order of magnitude as the accuracy of the present data. This is due to the low optical magnification which has been adjusted for the measurement of large plastic strains. However, beyond the yield point, a large volume expansion due to the opening of microcracks and crazes [8] can be clearly observed. It is noteworthy that the maximum value of about 20% in the neck under stress has never been suspected previously. Upon unloading, the volume strain decreases to about nil, in agreement with the few per cent to void content commonly reported from post-mortem density measurements on necked high-

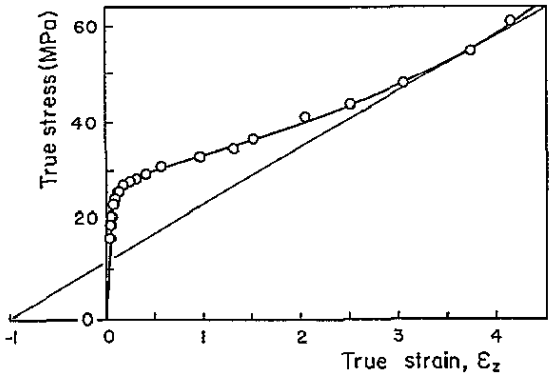

Figure 5. True-stress–true-strain curve. The straight line is the Considere construction having a slope equal to σ_N in the draw plateau.

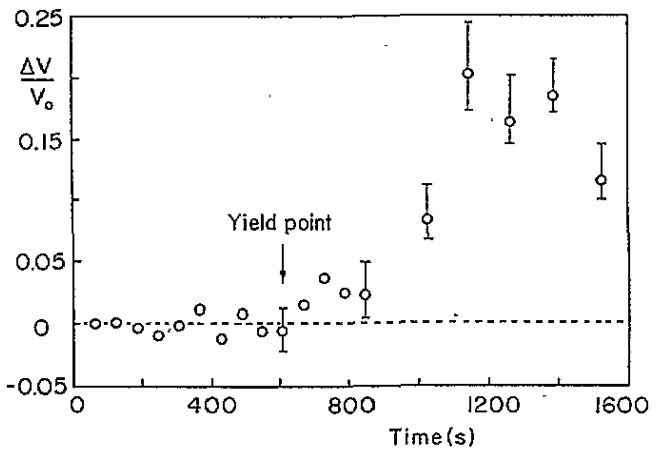

Figure 6. Volume strain as a function of time.

density polyethylenes. This is evidence that void opening is mainly a reversible process which emphasizes the role of the amorphous phase in the deformation process.

6. Conclusion

The present method of analysis of heterogeneous deformations provides true-strain measurements in thermoplastic flat films, along the three principal axes. Real-time determination of the volume variations accompanying the plastic deformation is also afforded.

This method is a contribution to the understanding of the tensile yield of strongly necking thermoplastic polymers. Precious information can be gained in addition to the classic nominal-stress–strain studies. Notably available is the correct characterization of the thermal activation of the elementary processes of plasticity.

The next step towards constant-true-strain-rate experiments is in progress.

Appendix

The basic relationship between the slope of an initially linear target, inclined with respect to the tensile axis, and the principal strains in the (x, z) plane of the sample front view (see figure 1) is established for the case of a heterogeneous deformation.

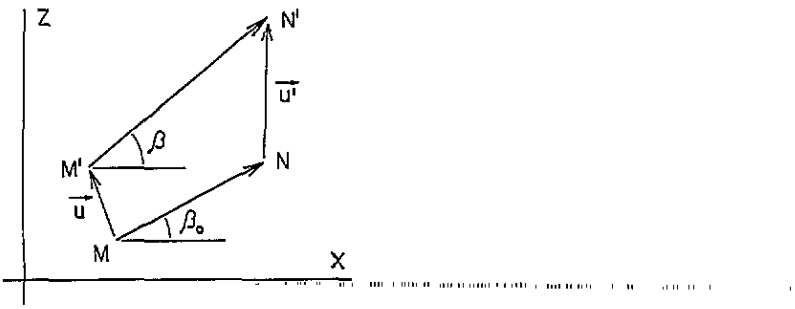

Figure A1. Geometrical transformation of an elementary vector of the sample front surface accompanying the deformation of the sample.

Let us consider the transformation, through any kind of deformation, of an elementary vector MN of the (x, y) plane into M'N' according to the scheme of figure A1. The various vectors of figure A1 have the following coordinates:

$$\overrightarrow{MN} = \begin{pmatrix} dx \\ dz \end{pmatrix} \qquad \vec{u} = \begin{pmatrix} u \\ v \end{pmatrix} \qquad \vec{u'} = \begin{pmatrix} u + du \\ v + dv \end{pmatrix} \qquad \overrightarrow{M'N'} = \begin{pmatrix} dx + du \\ dz + dv \end{pmatrix}.$$

Assuming that MN is an elementary vector of the target, a quite general form for the slope, $\tan \beta$, of the deformed target can be obtained by expressing the du and dv differentials with respect to the x and z coordinates

$$\frac{1}{\tan \beta} = \frac{dx + du}{dz + dv} = \frac{dx + (\partial u/\partial x)_z dx + (\partial u/\partial z)_x dz}{dz + (\partial v/\partial x)_z dx + (\partial v/\partial z)_x dz}. \tag{A1}$$

The longitudinal and transverse elongation strains are respectively given by

$$\epsilon_x = \left(\frac{\partial u}{\partial x}\right)_z \qquad \epsilon_z = \left(\frac{\partial v}{\partial z}\right)_x \tag{A2}$$

and the initial slope of the target is

$$\frac{1}{\tan \beta_0} = \frac{dx}{dz}. \tag{A3}$$

From figure A2, which shows the distortions of a square-mesh grid in the neck region of the copolymer drawn at room temperature, the following two pieces of experimental evidence have to be taken into account.

(1) The horizontal grid lines remain fairly well horizontal upon necking in agreement with previous reports on the plastic necking of high-density as well as low-density

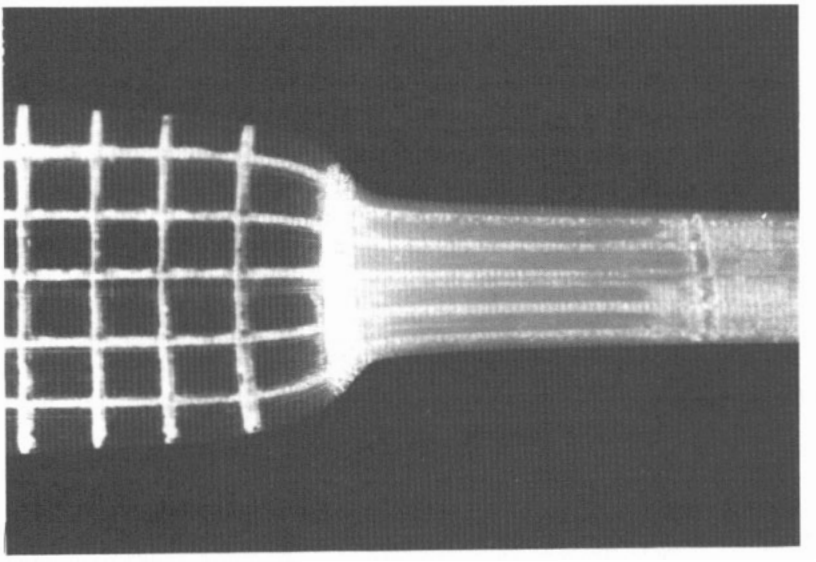

Figure A2. Photograph showing the distortions of a square-mesh grid along the neck shoulder (mesh dimension: 1.5 × 1.5 mm^2).

polyethylenes [9, 10]. This means that there is no or very little gradient of longitudinal displacement, i.e. longitudinal shear strain, in any cross-section of the neck. It implies

$$\left(\frac{\partial v}{\partial x}\right)_z = 0. \tag{A4}$$

(2) The vertical grid lines are distorted upon necking but remain equidistant. This is an indication that deformation is homogeneous over any cross-section of the neck and that the gradient of transverse displacements, i.e. the transverse shear strain, is purely affine. This can be formulated as

$$\left(\frac{\partial u}{\partial z}\right)_x = \frac{x}{x_e}\left(\frac{\partial u}{\partial z}\right)_{x_e} \tag{A5}$$

which means that, in every cross-section of z ordinate, the transverse shear strain at any x coordinate is proportional to the transverse shear strain at the sample edge of the abscissa x_e.

We have now to consider the transformation, under necking deformation, of an elementary vector of the edge of the front view of a sample having initially a uniform width, as shown in figure A3. Borrowing from the above analysis of the target deformation, we may assume

$$\overrightarrow{MN} = \begin{pmatrix} 0 \\ dz \end{pmatrix} \qquad \overrightarrow{M'N'} = \begin{pmatrix} du \\ dz + dv \end{pmatrix}.$$

Then, by analogy with (A1), and taking into account that $dx = 0$ and $x = x_e$ at the sample edge, we get the following expression for the slope, $\tan \alpha$, of the edge:

$$\frac{1}{\tan \alpha} = \frac{du}{dz + dv} = \frac{(\partial u/\partial z)_{x_e} dz}{dz + (\partial v/\partial z)_{x_e} dz} \tag{A6}$$

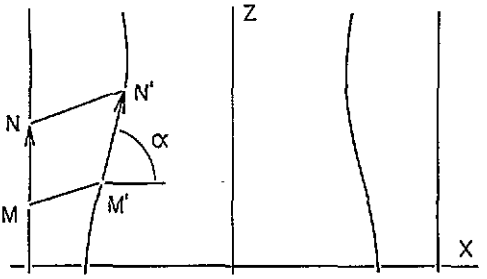

Figure A3. Geometrical transformation of an elementary vector of the sample edge in the necking region of the sample front view.

from which we obtain

$$\left(\frac{\partial u}{\partial z}\right)_{x_e} = \frac{1+\epsilon_z}{\tan\alpha}. \tag{A7}$$

(A1) can be finally reduced to the form

$$\frac{\tan\beta_0}{\tan\beta} - \frac{\tan\beta_0}{\tan\alpha}\frac{x}{x_e} = \frac{1+\epsilon_x}{1+\epsilon_z}. \tag{A8}$$

Note that the second term of the left-hand side of the equation (A8) accounts for the transverse shear strain along the z axis, due to the neck formation, which contributes to the target distortion. This term is nil for the three following situations:

(1) along the z axis, where $x = 0$, because the transverse-shear contributions from both sides of the neck are balanced for reasons of symmetry;

(2) in the particular case of plane-strain necking, because $\alpha = 90°$ in the front view and

(3) in the case of homogeneous deformation, because $\alpha = 90°$.

References

[1] G'Sell C and Jonas J J 1979 *J. Mater. Sci.* **14** 583
[2] G'Sell C, Boni S and Shrivastava S J 1983 *J. Mater. Sci.* **18** 903
[3] G'Sell C, Hiver J-M, Dahoun A and Souahi A 1992 *J. Mater. Sci.* **27** 5031
[4] G'Sell C and Marquez-Lucero A 1993 *Polymer* **34** 2740
[5] François Ph, Gloaguen J-M, Hue B and Lefebvre J-M 1994 *J. Physique* III **4** 321
[6] G'Sell C, Aly-Helal N A and Jonas J J 1983 *J. Mater. Sci.* **18** 1731
[7] Vincent P I 1960 *Polymer* **1** 7
[8] Friedrich K 1983 *Adv. Polym. Sci.* **52/53** 225
[9] Coates P D and Ward I M 1980 *J. Mater. Sci.* **15** 2897
[10] Mills P J, Hay J N and Haward R N 1985 *J. Mater. Sci.* **20** 501